J Mol Model (2013) 19:2143–2148
DOI 10.1007/s00894-012-1671-1

ORIGINAL PAPER

# Stability and electronic properties of 3D covalent organic frameworks

**Binit Lukose · Agnieszka Kuc · Thomas Heine**

Received: 1 July 2012 / Accepted: 29 October 2012 / Published online: 5 December 2012


**Abstract** Covalent organic frameworks (COFs) are a class of covalently linked crystalline nanoporous materials, versatile for nanoelectronic and storage applications. 3D COFs, in particular, have very large pores and low mass densities. Extensive theoretical studies of their energetic and mechanical stability, as well as their electronic properties, have been carried out for all known 3D COFs. COFs are energetically stable and their bulk modulus ranges from 3 to 20 GPa. Electronically, all COFs are semiconductors with band gaps corresponding to the HOMO–LUMO gaps of the building units.

**Keywords** Covalent organic frameworks · Density functional tight-binding · Bulk modulus · Band gap · HOMO–LUMO gap

## Introduction

Covalent organic frameworks (COFs) [1–3] comprise an emerging class of crystalline materials that combines organic functionality with nanoporosity. COFs have organic subunits stitched together by covalent entities including boron, carbon, nitrogen, oxygen or silicon atoms to form periodic frameworks with the faces and edges of molecular subunits exposed to pores. Hence, their applications can range from organic electronics to catalysis to gas storage and sieving [4–7]. The properties of COFs depend extensively on their molecular constituents and thus can be tuned by rational chemical design and synthesis [2, 8, 9]. Step by step reversible condensation reactions pave the way to accomplishing this target. Such a reticular approach allows prediction of the resulting materials and leads to long-range ordered crystal structures.

Since their first mention in the literature [1, 3], COFs have been under theoretical investigation [10–17], mainly for gas storage applications. Methods such as doping [18–24] and organic linker functionalization [25, 26] have been suggested to improve their storage capacities. In addition to their moderate pore size and internal surface area, COFs have the advantages of a low-weight material as they are made of light elements. Hence, their gravimetric adsorption capacity is remarkably high [10]. The lowest mass density ever reported for any crystalline material is that for COF-108 (0.18 g $cm^{-3}$). Also, their stronger covalent bonds, compared to related metal-organic frameworks (MOFs) [27], confer thermodynamic strength. These unique qualities of COFs make them attractive for hydrogen storage investigations.

Crystallization of linked organic molecules into 2D and 3D forms was achieved in 2005 [1] and 2007 [3], respectively, by the research group of O.M. Yaghi. Several COFs have been synthesized since then and some 2D COFs have proven useful for electronic or photovoltaic applications [4, 28–33]. However, other than some promising $H_2$ adsorption measurements [5, 34, 35] and a few synthetic improvements [7, 36–42], growth in this area appears to be slow compared to rapidly developing MOFs.

COF-102 and COF-103 were synthesized [3] by self-condensation of the non-planar tetra(4-dihydroxyborylphenyl)-methane (TBPM) and tetra(4-dihydroxyborylphenyl)silane (TBPS), respectively (see Fig. 1 for the building blocks and COF geometries). The co-condensation of these compounds with triangular hexahydroxytriphenylene (HHTP)

**Electronic supplementary material** The online version of this article (doi:10.1007/s00894-012-1671-1) contains supplementary material, which is available to authorized users.

B. Lukose (✉) · A. Kuc · T. Heine
Center for Functional Nanomaterials, School of Engineering and Science, Jacobs University Bremen, Campus Ring 1, 28759 Bremen, Germany
e-mail: b.lukose@jacobs-university.de

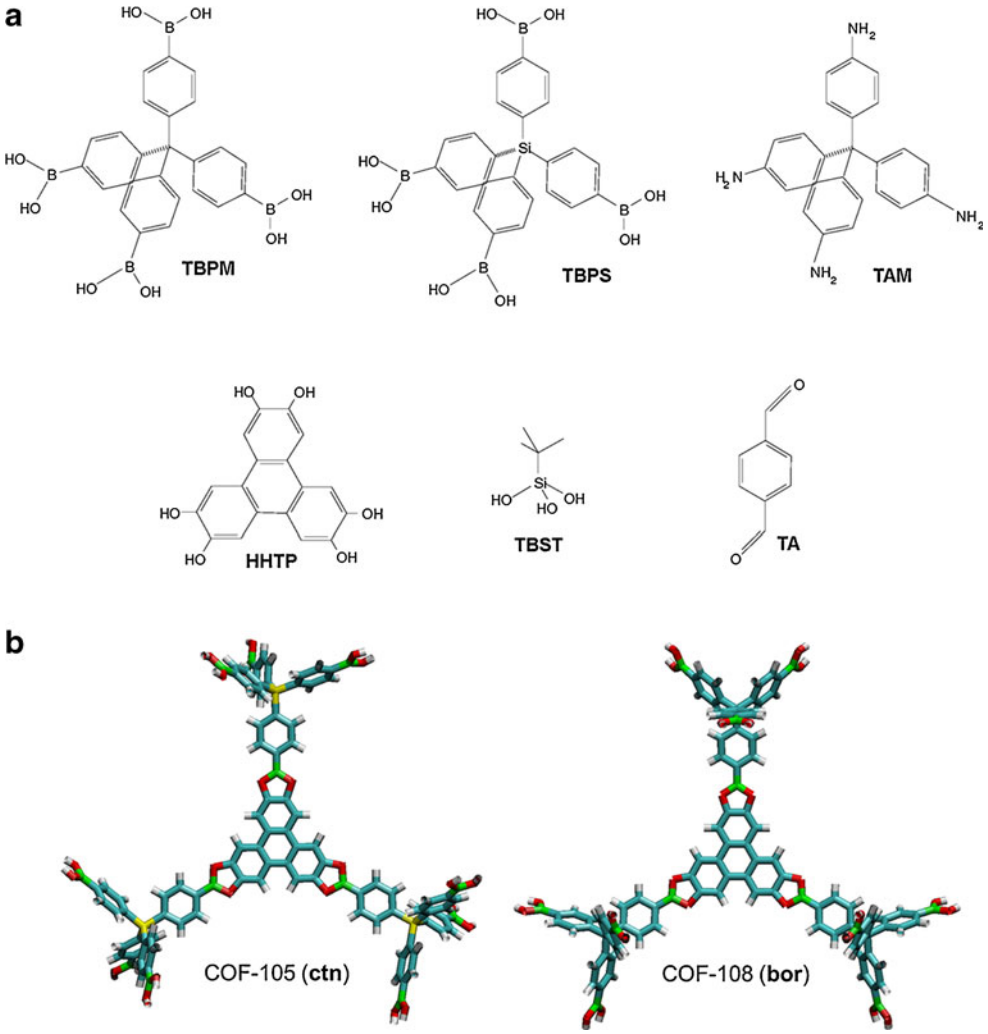


**Fig. 1** **a** Building blocks for the construction of 3D covalent organic frameworks (COFs). **b** Exemplary cluster models of COF-105 and COF-108. Both COFs are built of hexahydroxytriphenylene (HHTP) and tetra (4-dihydroxyborylphenyl)methane (TBPM) building blocks, but the relative orientation of phenyl rings leads to different topologies. Colors codes: *blue* C, *red* O, *green* B, *yellow* Si, *grey* H

results in COF-108 and COF-105, respectively, with different topologies. Yaghi et al. [3] have reported the formation of highly symmetric topologies: **ctn** (carbon nitride, $I\bar{4}3d$) and **bor** (boracite, $P\bar{4}3m$), when tetrahedral building blocks are linked together with triangular ones. Topology names were adopted from the reticular chemistry structure resource (RCSR) [43]. Simulated powder X-ray diffraction in comparison with experimental powder spectrum suggested **ctn** topology for COF-102, 103 and 105, and **bor** topology for COF-108. The condensation of tert-butylsilanetriol (TBST) and TBPM leads to the formation of COF-202 [44]. This was reported as **ctn** topology. The COF reactants and schematic diagrams of **ctn** and **bor** topologies are given in Fig. 1. The assembly of tetrahedral and linear units is very likely to result in a diamond-like form. COF-300 was formed by the condensation of tetrahedral tetra-(4-anilyl)-methane (TAM) and linear terephthaldehyde (TA) [45]. However, the synthesized structure was 5-fold interpenetrated **dia-c5** topology [43].

In this work, we present theoretical studies of 3D COFs using density functional based methods to explore their structural, electronic, energetic and mechanical properties. Our previous studies on 2D COFs [46, 47] questioned the stability of eclipsed arrangement of layers (AA stacking) and suggested energetically more stable serrated and inclined packing. In the present study, we attempted to explore the stability and electronic properties of the experimentally known 3D COFs, namely COF-102, 103, 105, 108, 202 and 300. Here, we follow the reticular assembly of the molecular units that form low-weight 3D COFs. In terms of the structural distinction from MOFs, COFs lack the versatility of metal ingredients, which results in diverse properties [48]. A collective study was carried out to investigate the characteristics and limitations of COFs.

## Methods

COF structures were fully optimized using the self-consistent charge-density functional based tight-binding (SCC-DFTB) level of theory [49, 50]. Two computational codes were used: deMonNano [51] and DFTB+[52]. The first code,

which has dispersion correction implemented to account for weak interactions [53], was used for geometry optimization and stability calculations. The second code, which can perform calculations using k-point sampling, was used to calculate the electronic properties (band structure and density of states). The number of k-points was determined by reaching convergence for the total energy as a function of k-points according to the scheme proposed by Monkhorst and Pack [54]. Periodic boundary conditions were used to represent frameworks of the crystalline solid state. A conjugate–gradient scheme was chosen for geometry optimization. An atomic force tolerance of $3\times10^{-4}$eV/Å was applied. The optimization, using Γ-point approximation, was performed on rectangular supercells containing more than 1,000 atoms. For validation of our method, we calculated energetic stability using density functional theory (DFT) at the PBE [55]/DZP [56] level as implemented in ADF code [57, 58] using cluster models. The cluster models contain a finite number of building units and correspond to the bulk topology of the COFs. XRD patterns were simulated using Mercury software [59, 60].

In this work, we continue to use the traditional nomenclature of the experimentally known COFs. All structures have the same tetrahedral blocks and differ only in the central $sp^3$ atom (carbon or silicon), as included in our nomenclature.

Bulk modulus (B) of a solid at absolute zero can be calculated as

$$B = V\frac{d^2E}{dV^2} \quad (1)$$

where $V$ and $E$ are the volume and energy, respectively.

COFs are formed in condensation reactions, where one water molecule is released per one bond created between the building blocks. The formation energy per bond, $E_{form}$, is calculated as follows:

$$E_{form} = E^{tot}/n + E_{H2O}{}^{tot} - (m_1E_{bb1}{}^{tot} + m_2E_{bb2}{}^{tot})/n, \quad (2)$$

where $E^{tot}$ is the total energy of the COF; $E_{H2O}{}^{tot}$ is the total energy of one free water molecule; $E_{bb1}{}^{tot}$ and $E_{bb2}{}^{tot}$ are total energies of interacting building blocks; $n$ is the number of bonds per unit cell; and $m_1$, $m_2$ are the numbers of building blocks 1 and 2, respectively.

## Results and discussion

### Structure and stability

Experimentally known 3D COF structures consist of tetrahedral building blocks with either $sp^3$ C or Si atoms in the central part. To extend our investigation into these structures, we aim to consider every 3D COF with both connecting atoms. In this work, we continue to use the well-established nomenclature for these materials; to distinguish modified structures with C or Si centers, we use the respective extensions '-C' or '-Si'.

The atomic positions and cell parameters of the COFs were optimized in the experimentally determined topologies. Optimized cell parameters in comparison with experimental values are given in Table 1. In general, calculated bond lengths of all studied COFs are C–B=1.50, C–C=1.39–1.44 (COF-300), C($sp^3$)-C=1.56, C–O=1.42, B–O=1.40, Si–C=1.88, Si–O=1.86, C–N=1.31–1.36 Å. These values agree within 6 % error with the experimental values [3, 44, 45]. Detailed analyses of the bond and dihedral angles show that the perfect tetrahedral building blocks with

**Table 1** Calculated cell parameters [Å], mass densities ρ [g cm$^{-3}$], band gaps Δ [eV], HOMO–LUMO gaps ($\Delta_{HL}$) of the building blocks [eV], bulk moduli B [GPa] and formation energies $E_{form}$ [kJ mol$^{-1}$] for all the studied 3D covalent organic frameworks (COFs). Experimental values are given in parenthesis. *HHTP* Hexahydroxytriphenylene, *TBPM* tetra(4-dihydroxyborylphenyl)methane, *TAM* tetrahedral tetra-(4-anilyl)-methane, *TAS* tetra-(4-anilyl)silane, *TA* terephthaldehyde

| Structure | Building blocks | Topology | Cell parameters | ρ | Δ [$\Delta_{HL}$] | B | $E_{form}$ |
|---|---|---|---|---|---|---|---|
| COF-021 | TBPM | **ctn** | 27.07 (27.17) | 0.43 | 3.9 [4.3] | 20.6 | −150.0 |
| COF-103 | TBPS | **ctn** | 28.17 (28.25) | 0.39 | 3.8 [4.1] | 13.9 | −145.5 |
| COF-105-C | TBPM, HHTP | **ctn** | 43.37 | 0.19 | 3.3 [4.3, 3.4] | 8.0 | −180.8 |
| COF-105 | TBPS, HHTP | **ctn** | 44.44 (44.89) | 0.18 | 3.2 [4.1, 3.4] | 7.9 | −170.6 |
| COF-108 | TBPM, HHTP | **bor** | 28.38 (28.40) | 0.17 | 3.2 [4.3, 3.4] | 3.7 | −179.8 |
| COF-108-Si | TBPS, HHTP | **bor** | 29.20 | 0.16 | 3.0 [4.1, 3.4] | 2.9 | −180.4 |
| COF-202 | TBPM, TBST | **ctn** | 30.47 (30.10) | 0.50 | 4.2 [4.3, 13.9] | 14.3 | −79.5 |
| COF-202-Si | TBPS, TBST | **ctn** | 31.57 | 0.46 | 3.9 [4.1, 13.9] | 15.3 | −76.3 |
| COF-300 | TAM, TA | **dia-c5** | 29.32, 9.25 (28.28, 10.08) | 0.49 | 2.3 [4.1, 2.6] | 14.4 | −402.9 |
| COF-300-Si | TAS, TA | **dia-c5** | 30.39, 9.59 | 0.44 | 2.3 [4.0, 2.6] | 13.3 | −399.3 |

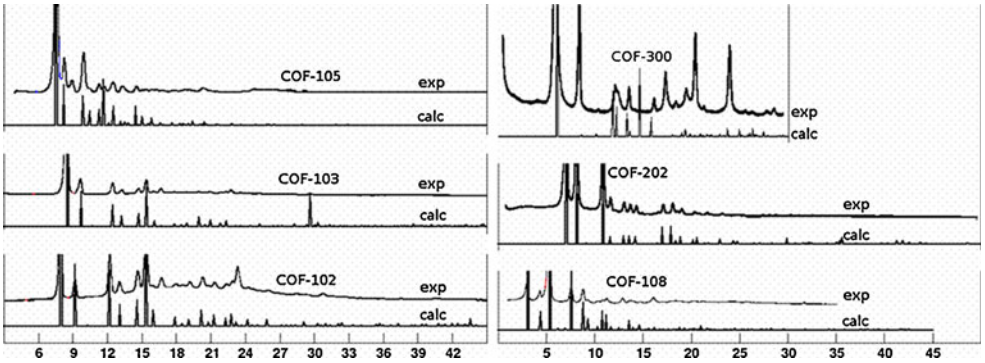


**Fig. 2** Simulated X-ray diffraction (XRD) of each COF compared with experimental patterns extracted from the literature [3, 44, 45]

109.5° for the C–C($sp^3$)/Si-C angle are found only for COFs -103 and -105. For all the other COFs, this angle deviates in the range of 102.5–113.0°. A much larger range of values was found for the dihedral C–C($sp^3$)/Si–C–C depending on the reference atoms taken into account (see crystal structures provided in the Supporting Information). The O–B–O bond angle in different boron-oxide rings agrees very well with experimental values: 113.2° (exp. 113.5°) in $C_2O_2B$ rings, 120.3° (exp. 122.8°) in $B_3O_3$ rings, and 121.7° (exp. 123.1°) in $B_2O_4Si_2$ rings. Despite some deviations in the angles, the symmetries of COFs are identical to the structures obtained experimentally.

Mass densities (see Table 1) of COFs range between 0.2 and 0.5 $g\,cm^{-3}$ and are smaller with silicon at the tetrahedral center. This implies that the presence of silicon atoms impacts more on the cell volume than on the total mass. That means that replacement of the $sp^3$ C with Si in COF-108 can change its mass density to a slightly lower value. To the best of our knowledge, among all the natural or synthesized crystals, COF-108 has the lowest mass density.

In order to validate our optimized structures, we simulated X-ray diffraction (XRD) of each COF and compared the results with the available experimental spectra (see Fig. 2). Almost all the simulated XRDs have excellent correlation in the peak positions with experimental peaks. Only COF-300 shows a somewhat significant difference in intensity. These differences may be attributed to the presence of guest molecules in the synthesized COF-300 [45].

The bulk modulus (B) is a measure of the mechanical stability of a material. The calculated values of B shown in Table 1 are larger than the force-field based calculation of B by Schmid et al. [61]. The B of COF-105 and COF-108 are relatively small compared with other COFs. Considering that these two COFs differ only in topology, it may be concluded that **ctn** nets are mechanically more stable compared to **bor**. COFs with carbon atoms in the center are mechanically more stable than those with silicon atoms. B values of COF-102, COF-103, COF-202 and interpenetrated COF-300 are higher than many of the isoreticular MOFs [62] and comparable to IRMOF-6 (12.41 GPa), MOF-5 (15.37 GPa) [63]. Non-interpenetrated COF-300 (single framework; **dia-a** topology [43]), however, has much lower bulk modulus of only 3.17 GPa, indicating that interpenetration can provide additional mechanical stability.

Formation energies calculated according to Eq. 2 are also given in Table 1. Condensation of monomers to form bulk 3D structures is exothermic in all the cases, supporting the reticular approach. The presence of C or Si at the vertex center does not show any particular trend in the formation energies. We calculated the formation energy of non-interpenetrated COF-300 (**dia-a**) to be −393.46 $kJ\,mol^{-1}$, which is comparable to the interpenetrated cases. For comparison, we performed DFT calculations at the PBE/DZP level as implemented in ADF code on finite structures. The cluster models consist of one triangular and three tetrahedral building units. The clusters are taken from the DFTB optimized periodic structures and their dangling bonds were saturated with H atoms. The obtained formation energies for COF-105-C, COF-105, COF-108, COF-108-Si are −99.4, −99.7, −124.5, −124.4 $kJ\,mol^{-1}$, respectively. These values are in reasonable agreement with the DFTB results. A comparison between COF-105 and COF-108 suggests that **bor** nets are energetically more favored than **ctn** nets. Substitution of the C($sp^3$) centers by Si does not influence network formation.

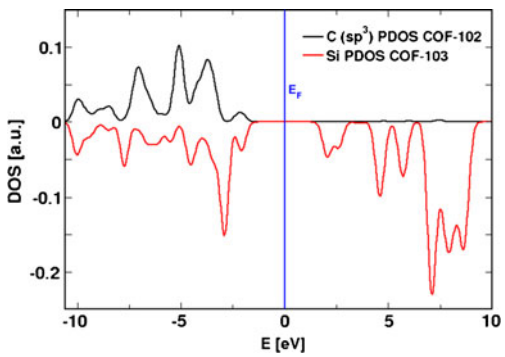


**Fig. 3** Partial density of states (DOS) of $sp^3$ C in COF-102 (*top*) and Si in COF-103 (*bottom*). The latter is inverted for comparison. The Fermi level $E_F$ is shifted to zero

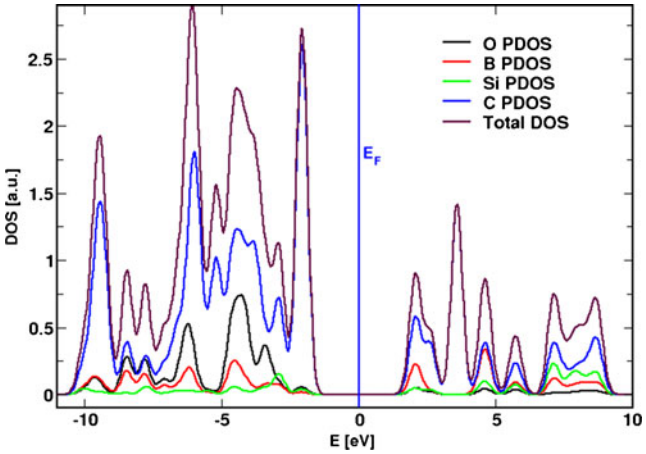


**Fig. 4** Partial and total density of states of COF-103. The Fermi level $E_F$ is shifted to zero

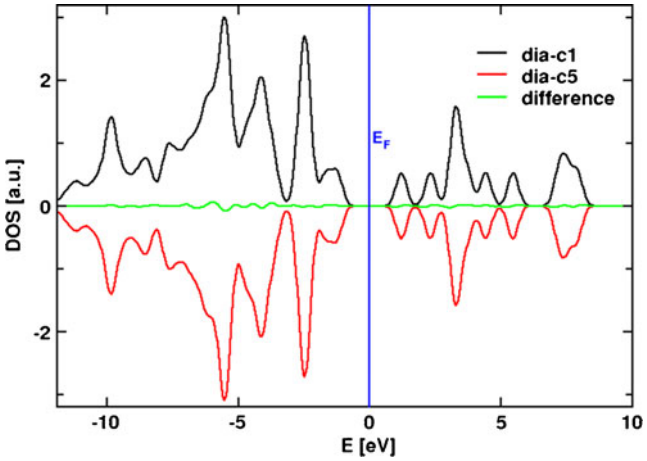


**Fig. 6** Density of states of non-interpenetrated (dia-c1) and 5-interpenetrated (dia-c5) COF-300

## Electronic properties

Band gaps (Δ) calculated for the 3D COFs are in the range of 2.3–4.2 eV (see Table 1), which show their semiconducting nature, similar to the hexagonal 2D COFs [47] and MOFs [62]. We obtained HOMO–LUMO gaps of 3.1 and 3.2 eV for the finite structures of COF-105 and -108, respectively, when calculated at the PBE/DZP level, in close agreement with the DFTB band gaps. The band gap decreases with the increase of conjugated rings in the unit cell relative to the number of other atoms. We obtained similar results for 2D COFs [47]. Compared with carbon atoms, Si atoms at the tetrahedral centers give a relatively smaller Δ. This is evident from the partial density of states of C ($sp^3$) in COF-102 and Si in COF-103 plotted in Fig. 3. Carbon atoms define the band edges of the partial density of states (PDOS; see Fig. 4). The band gaps of COF-105 and COF-108 differ only slightly (see Fig. 5), which means that the band gap is nearly independent of the topology. This is because for each atom, the coordination number and the neighboring atoms remain the same in both **ctn** and **bor** networks, despite their difference in topology. DOS of non-interpenetrated (**dia-a**) and 5-fold interpenetrated (**dia-c5**) COF-300 are plotted in Fig. 6. It may be concluded from their negligible differences that interpenetration does not alter the DOS of a framework.

We calculated the HOMO–LUMO gaps of the molecular building blocks (see Table 1). In comparison, band gaps of COFs are slightly smaller than the smallest of the HOMO–LUMO gaps of the building units.

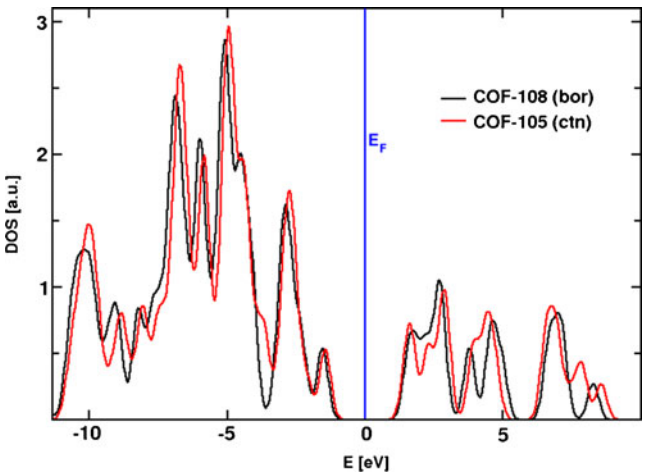


**Fig. 5** Density of states of COF-108 (bor) and COF-105 (ctn). The two COFs differ only in topology

## Conclusions

In summary, we have calculated the energetic, mechanical and electronic properties of all known 3D COF using the DFTB method. Formation of 3D COFs is energetically favorable, supporting the reticular chemistry approach. Mechanical stability is in line with other framework materials, *e.g.* MOFs, and bulk modulus does not exceed 20 GPa. Also, all COFs are semiconducting with band gaps ranging from 2 to 4 eV. Band gaps are analogous to the HOMO–LUMO gaps of the molecular building units. We believe that this extensive study will define the place of COFs in the broad area of nanoporous materials, and that the information obtained from this work will help the strategic development and modification of porous materials for targeted applications.

## References

1. Cote AP, Benin AI, Ockwig NW, O'Keeffe M, Matzger AJ, Yaghi OM (2005) Science 310(5751):1166–1170
2. Cote AP, El-Kaderi HM, Furukawa H, Hunt JR, Yaghi OM (2007) J Am Chem Soc 129:12914–12915

3. El-Kaderi HM, Hunt JR, Mendoza-Cortes JL, Cote AP, Taylor RE, O'Keeffe M, Yaghi OM (2007) Science 316(5822):268–272
4. Wan S, Guo J, Kim J, Ihee H, Jiang DL (2008) Angew Chem Int Ed 47(46):8826–8830
5. Furukawa H, Yaghi OM (2009) J Am Chem Soc 131(25):8875–8883
6. Keskin S (2012) J Phys Chem C 116(2):1772–1779
7. Ding S-Y, Gao J, Wang Q, Zhang Y, Song W-G, Su C-Y, Wang W (2011) J Am Chem Soc 133(49):19816–19822
8. Ockwig NW, Delgado-Friedrichs O, O'Keeffe M, Yaghi OM (2005) Acc Chem Res 38(3):176–182
9. Yaghi OM, O'Keeffe M, Ockwig NW, Chae HK, Eddaoudi M, Kim J (2003) Nature 423(6941):705–714
10. Tylianakis E, Klontzas E, Froudakis GE (2011) Nanoscale 3 (3):856–869
11. Assfour B, Seifert G (2010) Microporous Mesoporous Mater 133 (1–3):59–65
12. Schmid R, Tafipolsky M (2008) J Am Chem Soc 130(38):12600–12601
13. Garberoglio G, Vallauri R (2008) Microporous Mesoporous Mater 116(1–3):540–547
14. Han SS, Mendoza-Cortes JL, Goddard WA (2009) Chem Soc Rev 38(5):1460–1476
15. Tylianakis E, Klontzas E, Froudakis GE (2009) Nanotechnology 20:9
16. Klontzas E, Tylianakis E, Froudakis GE (2008) J Phys Chem C 112(24):9095–9098
17. Garberoglio G (2007) Langmuir 23:12154–12158
18. Lan JH, Cao DP, Wang WC (2010) J Phys Chem C 114(7):3108–3114
19. Lan JH, Cao DP, Wang WC, Smit B (2010) ACS Nano 4(7):4225–4237
20. Li F, Zhao JJ, Johansson B, Sun LX (2010) Int J Hydrogen Energy 35(1):266–271
21. Wu MM, Wang Q, Sun Q, Jena P, Kawazoe Y (2010) J Chem Phys 133:154706
22. Choi YJ, Lee JW, Choi JH, Kang JK (2008) Appl Phys Lett 92:173102
23. Zou XL, Zhou G, Duan WH, Choi K, Ihm J (2010) J Phys Chem C 114(31):13402–13407
24. Klontzas E, Tylianakis E, Froudakis GE (2009) J Phys Chem C 113(50):21253–21257
25. Klontzas E, Tylianakis E, Froudakis GE (2010) Nano Lett 10 (2):452–454
26. Tilford RW, Mugavero SJ, Pellechia PJ, Lavigne JJ (2008) Adv Mater 20(14):2741–2746
27. Li H, Eddaoudi M, O'Keeffe M, Yaghi OM (1999) Nature 402 (6759):276–279
28. Feng X, Chen L, Honsho Y, Saengsawang O, Liu L, Wang L, Saeki A, Irle S, Seki S, Dong Y, Jiang D (2012) Adv Mater 24(22):3026–3031
29. Feng X, Liu L, Honsho Y, Saeki A, Seki S, Irle S, Dong Y, Nagai A, Jiang D (2012) Angew Chem Int Ed 51(11):2618–2622
30. Wan S, Guo J, Kim J, Ihee H, Jiang DL (2009) Angew Chem Int Ed 48(30):5439–5442
31. Spitler EL, Dichtel WR (2010) Nat Chem 2:672–677
32. Ding XS, Guo J, Feng XA, Honsho Y, Guo JD, Seki S, Maitarad P, Saeki A, Nagase S, Jiang DL (2011) Angew Chem Int Ed 50 (6):1289–1293
33. Wan S, Gandara F, Asano A, Furukawa H, Saeki A, Dey SK, Liao L, Ambrogio MW, Botros YY, Duan X, Seki S, Stoddart JF, Yaghi OM (2011) Chem Mater 23(18):4094–4097
34. Han SS, Furukawa H, Yaghi OM, Goddard WA III (2008) J Am Chem Soc 130(35):11580–11581
35. Mendoza-Cortes JL, Han SS, Furukawa H, Yaghi OM, Goddard WA III (2010) J Phys Chem A 114(40):10824–10833
36. Colson JW, Woll AR, Mukherjee A, Levendorf MP, Spitler EL, Shields VB, Spencer MG, Park J, Dichtel WR (2011) Science 332 (6026):228–231
37. Tilford RW, Gemmill WR, zur Loye H-C, Lavigne JJ (2006) Chem Mater 18(22):5296–5301
38. Blunt MO, Russell JC, Champness NR, Beton PH (2010) Chem Commun 46(38):7157–7159
39. Berlanga I, Ruiz-Gonzalez ML, Gonzalez-Calbet JM, Fierro JLG, Mas-Balleste R, Zamora F (2011) Small 7(9):1207–1211
40. Bunck DN, Dichtel WR (2012) Angew Chem Int Ed 51(8):1885–1889
41. Nagai A, Guo Z, Feng X, Jin S, Chen X, Ding X, Jiang D (2011) Nat Commun 2:536
42. Kalidindi SB, Yusenko K, Fischer RA (2011) Chem Commun 47 (30):8506–8508
43. O'Keeffe M, Peskov MA, Ramsden SJ, Yaghi OM (2008) Acc Chem Res 41(12):1782–1789
44. Hunt JR, Doonan CJ, LeVangie JD, Cote AP, Yaghi OM (2008) J Am Chem Soc 130(36):11872–11873
45. Uribe-Romo FJ, Hunt JR, Furukawa H, Klock C, O'Keeffe M, Yaghi OM (2009) J Am Chem Soc 131(13):4570–4571
46. Lukose B, Kuc A, Heine T (2011) Chem Eur J 17(8):2388–2392
47. Lukose B, Kuc A, Frenzel J, Heine T (2010) Beilstein J Nanotechnol 1:60–70
48. Lukose B, Supronowicz B, Petkov PS, Frenzel J, Kuc A, Seifert G, Vayssilov GN, Heine T (2011) Phys Stat Sol b249(2):335–342
49. Oliveira AF, Seifert G, Heine T, Duarte HA (2009) J Braz Chem Soc 20(7):1193–1205
50. Seifert G, Porezag D, Frauenheim T (1996) Int J Quantum Chem 58(2):185–192
51. Heine T, Rapacioli M, Patchkovskii S, Frenzel J, Koester AM, Calaminici P, Escalante S, Duarte HA, Flores R, Geudtner G, Goursot A, Reveles JU, Vela A, Salahub DR (2009) deMon-nano. deMon-nano edn. edn. deMon,
52. DFTB+- Density Functional based Tight binding (and more), BCCMS, Bremen, Germany. Web: http://www.dftb-plus.info/
53. Zhechkov L, Heine T, Patchkovskii S, Seifert G, Duarte HA (2005) J Chem Theor Comput 1(5):841–847
54. Monkhorst HJ, Pack JD (1976) Phys Rev B 13(12):5188–5192
55. Perdew JP, Burke K, Ernzerhof M (1996) Phys Rev Lett 77 (18):3865–3868
56. Van Lenthe E, Baerends EJ (2003) J Comput Chem 24(9):1142–1156
57. Velde GT, Bickelhaupt FM, Baerends EJ, Guerra CF, Van Gisbergen SJA, Snijders JG, Ziegler T (2001) J Comput Chem 22(9):931–967
58. ADF2009.01,SCM,Theoretical Chemistry VU (2009) Amsterdam, The Netherlands
59. Macrae CF, Edgington PR, McCabe P, Pidcock E, Shields GP, Taylor R, Towler M, van De Streek J (2006) J Appl Crystallogr 39:453–457
60. http://www.ccdc.cam.ac.uk/products/mercury/ Mercury—Crystal Structure Visualisation and Exploration Made Easy. Cambridge Crystallographic Data Centre. http://www.ccdc.cam.ac.uk/products/mercury/
61. Amirjalayer S, Snurr RQ, Schmid R (2012) J Phys Chem C 116 (7):4921–4929
62. Kuc A, Enyashin A, Seifert G (2007) J Phys Chem B 111 (28):8179–8186
63. Yang LM, Vajeeston P, Ravindran P, Fjellvag H, Tilset M (2010) Inorg Chem 49(22):10283–10290